



CHORUS

This is the accepted manuscript made available via CHORUS. The article has been published as:

Fermi-surface topology and low-lying electronic structure of the iron-based superconductor

$\text{Ca}_{10}(\text{Pt}_3\text{As}_8)(\text{Fe}_2\text{As}_2)_5$

Madhab Neupane, Chang Liu, Su-Yang Xu, Yung-Jui Wang, Ni Ni, J. M. Allred, L. A. Wray, N.

Alidoust, Hsin Lin, R. S. Markiewicz, A. Bansil, R. J. Cava, and M. Z. Hasan

Phys. Rev. B **85**, 094510 — Published 20 March 2012

DOI: [10.1103/PhysRevB.85.094510](https://doi.org/10.1103/PhysRevB.85.094510)

Fermi surface topology and low-lying electronic structure of a new iron-based superconductor $\text{Ca}_{10}(\text{Pt}_3\text{As}_8)(\text{Fe}_2\text{As}_2)_5$

Madhab Neupane,¹ Chang Liu,¹ Su-Yang Xu,¹ Yung-Jui Wang,² Ni Ni,³ J. M. Allred,³ L. A. Wray,^{1,4} N. Alidoust,¹ Hsin Lin,² R. S. Markiewicz,² A. Bansil,² R. J. Cava,³ and M. Z. Hasan¹

¹*Joseph Henry Laboratory and Department of Physics,
Princeton University, Princeton, New Jersey 08544, USA*

²*Department of Physics, Northeastern University, Boston, Massachusetts 02115, USA*

³*Department of Chemistry, Princeton University, Princeton, New Jersey 08544, USA*

⁴*Advanced Light Source, Lawrence Berkeley National Laboratory, Berkeley, California 94305, USA*

(Dated: February 17, 2012)

We report a study of low energy electronic structure and Fermi surface topology for the recently discovered iron-based superconductor $\text{Ca}_{10}(\text{Pt}_3\text{As}_8)(\text{Fe}_2\text{As}_2)_5$ (the 10-3-8 phase, with $T_c \sim 8$ K), via angle resolved photoemission spectroscopy (ARPES). Despite its triclinic crystal structure, ARPES results reveal a fourfold symmetric band structure with the absence of Dirac-cone-like Fermi dots (related to magnetism) found around the Brillouin zone corners in other iron-based superconductors. Considering that the triclinic lattice and structural supercell arise from the Pt_3As_8 intermediary layers, these results indicate that those layers couple only weakly to the FeAs layers in this new superconductor at least near the surface, which has implications for the determination of its potentially novel pairing mechanism.

PACS numbers: 74.25.Jb, 74.70.Dd, 79.60.Bm

I. INTRODUCTION

The recent discovery and characterization of new superconducting phases in the Ca-Fe-Pt-As system $\text{Ca}_{10}(\text{Pt}_n\text{As}_8)(\text{Fe}_2\text{As}_2)_5$ (Refs. 1–4) has potentially significant impact on the field of iron-based high- T_c superconductors.^{5–12} Most importantly, these new phases serve as ideal platforms for systematic studies of the physics of the intermediary layers and their impact on the superconducting properties - an important yet open question in the field of arsenide superconductivity. In high- T_c cuprates,^{13–17} such a study is made possible by the availability of materials such as the $\text{Bi}_2\text{Sr}_2\text{Ca}_{n-1}\text{Cu}_n\text{O}_{2n+4+x}$ ($n = 1 - 3$) series,^{16,17} within which one finds a drastic correlation between the number of intermediary layers and the superconducting transition temperature (T_c). In the iron pnictides, a similar type of survey has previously been unavailable due to the lack of appropriate systems: one needs to search for a series of stoichiometric materials with different but systematically adjusted chemical compositions in either the iron-containing layers or the intermediary layers. The unique crystal structures in the Ca-Fe-Pt-As systems, on the other hand, yield drastically different symmetries and periodicities for the layers of FeAs tetrahedra and the intermediary layers. Therefore, the intralayer (hopping within the FeAs layers) and interlayer (hopping between the FeAs and Ca-Pt-As layers) contribution to the density of states at the Fermi level (E_F) can be uniquely distinguished. Studies of the electronic structure of the Ca-Fe-Pt-As system are thus of crucial importance toward the understanding of the interlayer physics and the microscopic mechanism of high- T_c superconductivity in the iron pnictides.

In this paper, we report a study of the electronic structure of the Ca-Fe-Pt-As system for $n = 3$ [the 10-3-8

phase with $T_c \sim 8$ K] using angle resolved photoemission spectroscopy (ARPES) as well as first principles calculations. ARPES measurements reveal the three dimensional Fermi surface topology and the band structure close to E_F . We observe well defined Fermi surfaces with *tetragonal* symmetry that are similar to those of other iron-based superconductors, even though arising from an unambiguously triclinic crystal structure with a larger in-plane unit cell. First principles band calculations find very small contribution of the platinum density of states at E_F for the 10-3-8 phase. These results are indicative of a weak interlayer hopping between the FeAs and the PtAs intermediary layers in this Ca-Fe-Pt-As system.

II. METHODS

High-quality single crystals of the 10-3-8 phase used in this study were grown by conventional flux method.² ARPES measurements were performed in the Synchrotron Radiation Center (SRC), Wisconsin using a VG-Scienta R4000 electron analyzer. Energy resolution was set to 10-30 meV. Samples were cleaved *in situ* and measured at 10-30 K under a vacuum condition better than 4×10^{-11} torr. The samples were found to be very stable and without degradation for the typical measurement period of 20 hours. First principles calculations are based on the density functional theory (DFT) framework plus the local density approximation (LDA), the Ceperley-Alder exchange-correlation functional¹⁸ and projector augmented wave method,¹⁹ all implemented in the VASP package.²⁰ The crystal structure of the 10-3-8 phase is taken from Ref. 2 and the off- (Pt_3As_8) Pt atom is assigned to a position above the (Pt_3As_8) plane.² The self-consistency of bulk calculation is done with $8 \times 8 \times 8$ k -

point mesh. For in-plane Fermi surface calculation, the k -mesh is increased to 201×201 in the k_x - k_y plane. The total energy convergence with respect to the k -point is 0.3 meV per atom. The kinetic energy cutoff is 280 eV.

III. RESULTS AND DISCUSSION

We begin our discussion with a detailed examination of the crystallographic properties of the 10-3-8 single crystal, as summarized in Fig. 1. This crystal has a triclinic unit cell with primitive vectors of length $a = b = 8.759$ Å, $c = 10.641$ Å, $\alpha = 94.744^\circ$, $\beta = 104.335^\circ$, and $\gamma = 90.044^\circ \simeq 90^\circ$ (Ref. 2) [see Fig. 1(a)-(c) for definitions]. Markedly, such a triclinic atomic arrange-

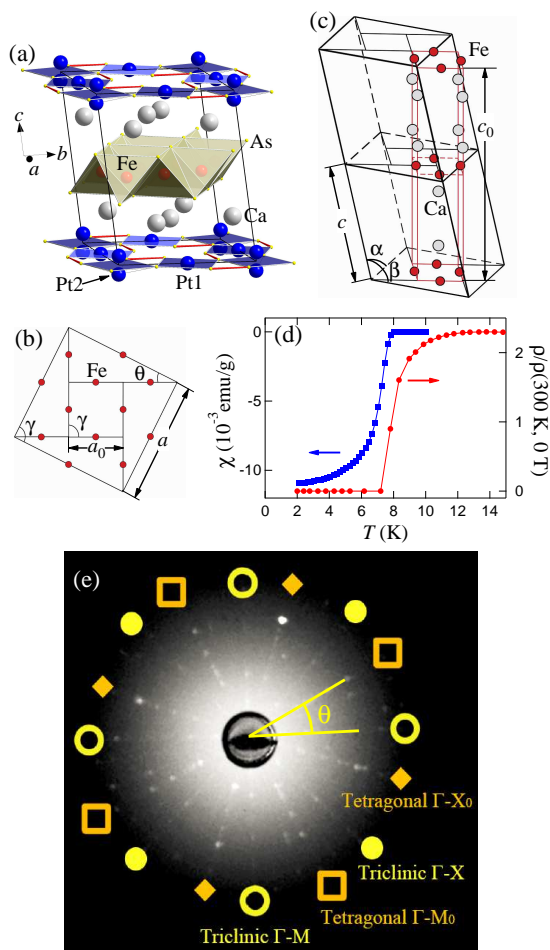


FIG. 1: (Color online) Crystallographic and superconducting properties of $\text{Ca}_{10}(\text{Pt}_3\text{As}_8)(\text{Fe}_2\text{As}_2)_5$ (10-3-8). (a) Crystal structure of the 10-3-8 phase. (b)-(c) Schematic crystal structure in (b) the a - b plane and (c) three dimensions. (d) Low temperature resistivity (right axis) and magnetic susceptibility (left axis) for the 10-3-8 phase. (e) Laue picture of a 10-3-8 single crystal. Reflection peaks for both the triclinic (yellow circles) and tetragonal (orange squares) lattices are clearly observed.

ment is experienced only by the platinum atoms in the crystal; the calcium atoms and the FeAs_4 tetrahedra arrange in a tetragonal fashion with lattice parameters $a_0 = b_0 = 3.917$ Å, $c_0 = 20.548$ Å. From Fig. 1(b) one notices that the in-plane triclinic unit cell is essentially a $\sqrt{5}$ superlattice that forms along the (210) direction of the tetragonal cell, making an in-plane inclusion angle of $\theta = \arctan(1/2) = 26.56^\circ$ and a length relation $a = \sqrt{5}a_0$ between the two lattices. Fig. 1(c) reveals that the top and bottom surface centers of the triclinic unit cell displace horizontally via an in-plane vector $(a_0/2, a_0/2)$. Therefore, the height of the tetragonal cell measures $c_0 = 2\sqrt{c^2 - a_0^2/2} = 20.548$ Å, and, if the interlayer hopping between the PtAs and FeAs layers is weak, the ARPES Fermi surface should reflect a similar topology to the other prototype pnictides, with possibly weak FeAs shadow bands associated with superlattice folding and additional features associated with the PtAs layer. Fig. 1(d) presents the superconducting properties of the 10-3-8 single crystals used for ARPES measurements. Both the resistivity and magnetic susceptibility data show clear signature of superconductivity at $T_c \sim 8$ K. The transition width in temperature is less than 3 K, indicating high quality and spatial homogeneity for the as-grown crystals.

Fig. 1(e) shows the x-ray Laue picture of a 10-3-8 crystal. Reflection peaks are clearly resolved and corresponding high symmetry directions are marked and labeled. It is very important to point out here that crystal twinning effect is unlikely to hinder the ARPES observation of the PtAs superlattice. It is true that a sufficiently large crystal must contain structural domains in which the triclinic superlattice is rotated by either θ or $-\theta$ with respect to the tetragonal lattice. Thus, the ARPES signal for the triclinic PtAs lattice contains ingredient from both domains, and the intensity for signal from each domain is weakened. We argue here, based on the x-ray Laue picture, that this effect should not be the main reason for the invisibility of the ARPES superlattice signal. In Fig. 1(e), reflection peaks for the triclinic lattice (yellow circles) are clearly observed at a clockwise angle of θ ($\pm 0.1^\circ$ accuracy) with respect to the tetragonal lattice (orange squares). In the counterclockwise angle of θ , however, reflection peaks are not present (or the intensity is very weak). This observation points out that the domains may have a preferred orientation, which limits the possible influence on the ARPES visibility. We further state here that, even if there is no preferred orientation for the structural domains, ARPES signal for both domains shall still be visible given a large enough interlayer hopping, since these domains are well defined by bright peaks in x-ray diffraction. Therefore, the corresponding ARPES intensity will be comparable to that of the tetragonal lattice.

We now present the ARPES data for the Fermi surface topology of the 10-3-8 phase. Fig. 2(a) shows the Fermi surface plots for four different photon energies. The circular/diamond-shaped α_1/α_2 Fermi pockets

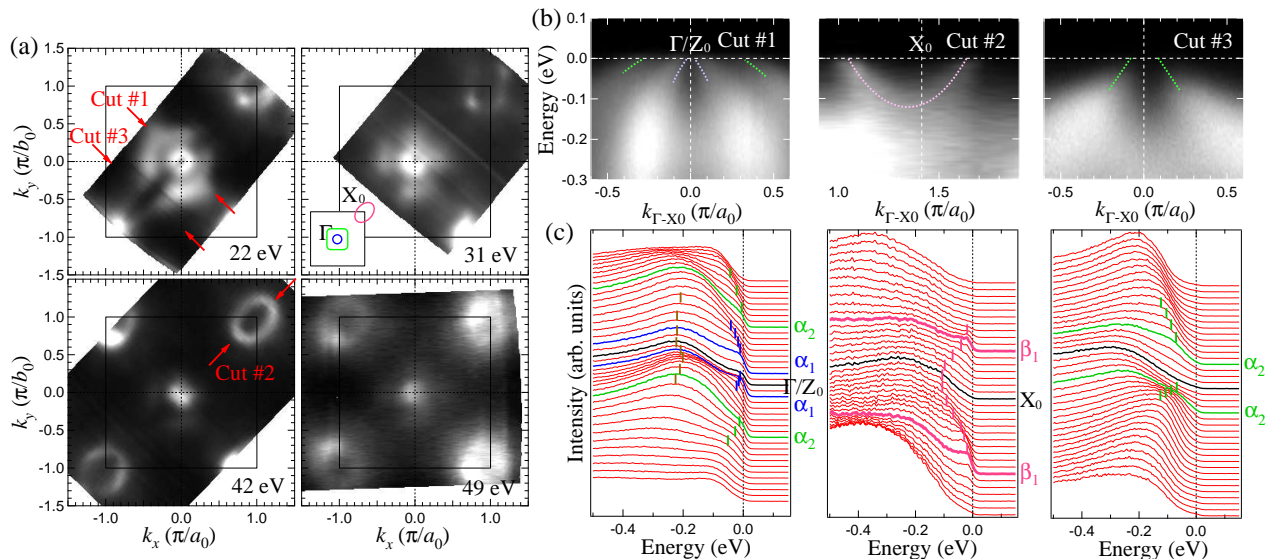


FIG. 2: (Color online) ARPES Fermi surface maps and k - E cuts for selected incident photon energies. (a) Fermi surface maps for four different photon energies (lower right corner in each panel). Inset of the 31 eV panel shows definition of high symmetry points and a schematic in-plane electronic structure. Brillouin zone sizes are determined based on the tetragonal cell [see Fig. 3(c) for relations between momenta in the triclinic and tetragonal cells]. (b) Raw k - E maps and (c) corresponding energy distribution curves along directions marked by Cut #1 - #3 in Fig. 2(a). The two hole pockets around Γ/Z_0 and the electron pocket around X_0 are labeled as α_1 , α_2 , and β_1 , respectively and are tracked with blue (dark grey), green (medium grey), and pink (light grey) colors in Fig. 2(b)-(c).

around the zone center as well as the elliptical β_1 Fermi pocket around the zone corners are clearly observed. Raw ARPES intensity maps in Fig. 2(b) and the corresponding energy distribution curves (EDCs) in Fig. 2(c) (Cuts #1 and #2) verify the holelike nature of the α_1 and α_2 bands and the electronlike nature of the β_1 band. There is a less dispersive but clearly visible band at a binding energy of ~ 0.2 eV [tracked by brown markers in Fig. 2(c)]. First principle calculation shows a considerable contribution of the Pt d -orbitals to the total density of states (DOS) at about 0.2-0.3 eV below E_F . Thus, this band may be influenced to some extent by the Pt $5d$ orbitals. Fig. 2(a) also reveals that the shape and sizes of the X electron pockets at the Brillouin zone corners are different than those of the observed holelike Fermi surfaces at the zone center. As a result, nesting condition among these Fermi surfaces is not perfect. Based on the ARPES k - E maps [Fig. 2(b)], we also calculate the Fermi velocities for the three Fermi crossing bands α_1 , α_2 , and β_1 . The values are: $v_F(\alpha_1) \sim 0.494$ eV \AA , $v_F(\alpha_2) \sim 0.182$ eV \AA , and $v_F(\beta_1) \sim 0.587$ eV \AA , which are very similar to the ones obtained for BaFe₂As₂ (Ref. 29).

In Fig. 3 we present the variation of the electron and hole pockets with photon energy, i.e., dispersion along the k_z axis of the BZ of the tetragonal lattice. Fig. 3(a) shows the k_z dispersion data (Fermi surface map in the Γ - X - Z plane). In Fig. 3(b) we plot the momentum distribution curves (MDCs) at E_F for each photon energy. The variation of α_1 and α_2 Fermi pockets is tracked by

blue and green markers. In Fig. 3(d) we plot the raw ARPES k - E maps across the zone center at selected photon energies (k_z values). The presence of multiple Fermi crossings is further verified by the MDCs (yellow curves at the top of each intensity plot) at E_F . The inner holelike Fermi surface (α_1) shows considerable k_z dispersion. In particular, the α_1 pocket is essentially closed at k_z values 19.4 and 20.6 π/c_0 , while the two MDC peaks at other k_z values signify its opening. This dispersive pattern results in ellipsoidal Fermi pockets with a periodicity of $4\pi/c_0$. These observations are captured in the schematic three dimensional Fermi surface [Fig. 3(c)]. It is worthwhile to point out that the observation of k_z dispersion proves the bulk sensitivity for the ARPES data in this compound. For other Fermi crossing bands, a weak intensity variation is observed for the α_2 pocket and almost no k_z dispersion is observed for the β_1 pockets, indicating the quasi two dimensional nature of these bands.

The most important observation from Figs. 2 and 3 is that the ARPES electronic structure has a *tetragonal* symmetry, and the experimental Brillouin zone size is proportional to π/a_0 rather than π/a in the k_x - k_y plane [Fig. 2(a)]. In other words, the ARPES signal reveals that the electronic system is tetragonal, with the periodicity of the FeAs layer sublattice. This observation is noteworthy for two reasons. First, it points out directly that the triclinic arrangement and larger supercell periodicity of the platinum atoms have very little influence on the electronic structure - if the platinum orbitals had a strong contribution at E_F , then the observa-

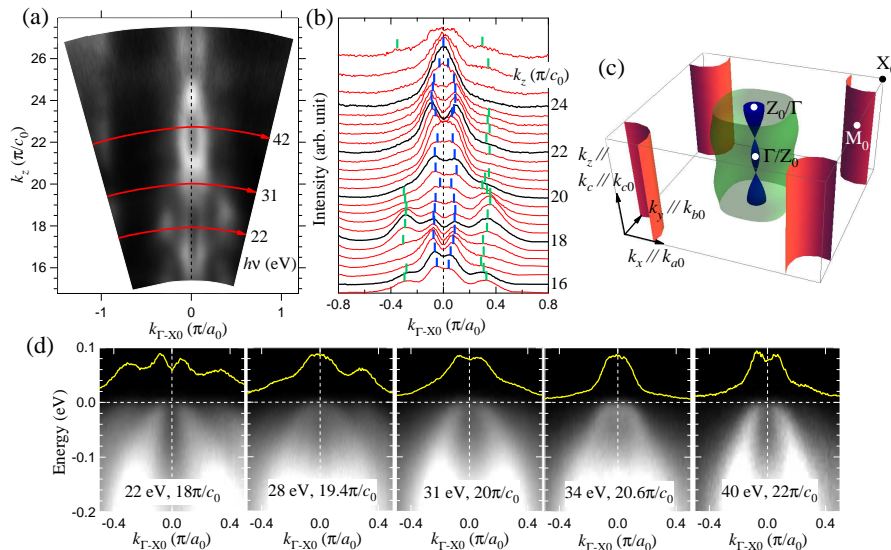


FIG. 3: (Color online) Analysis of k_z dispersion data. (a) k_z dispersion data for the 10-3-8 phase, taken along the Γ - X_0 direction with photon energies 15 to 64 eV. Inner potential is set to 9.5 eV. (b) Momentum distribution curves (MDCs) for different k_z values. Fermi crossing bands are marked with the same colors as in Fig. 2. (c) Schematics of an experiment-derived Fermi surface construction in three dimensions. (d) Raw ARPES k - E maps across the zone center ($k = 0$) for selected photon energies. Yellow (light grey) curves are MDCs at E_F . The α_1 band evolves below E_F around 19.4 and 20.6 π/c_0 and crosses E_F for other photon energies, forming a bigger ellipsoidal hole pocket centering at Z_0/Γ and a smaller hole pocket centering at Γ/Z_0 .

tion of Fermi pockets arranged according to the triclinic Brillouin zone is expected. From this we deduce that the hybridization between bands from the PtAs intermediary layers and those from the FeAs layers has to be weak. Although this is only a qualitative statement, the unique crystal structure of the 10-3-8 phase does provide an important estimation of the interlayer hopping strength that is otherwise hard to obtain from experiment in the FeAs superconductors: interlayer hopping must be so weak that it renders the triclinic lattice invisible by photoemission. Second, the ARPES electronic structure mimics the electronic structures of other prototype pnictides like $A\text{EFe}_2\text{As}_2$ (“122”, $A\text{E} = \text{Ca}, \text{Sr}, \text{Ba}, \text{etc.}$). Not only the in-plane lattice parameter a_0 but also the shapes, sizes and Fermi velocities of the Γ and X_0 Fermi pockets show very little difference with those of the 122 parent compounds.^{21–29} This indicates that a universal electronic structure capturing the underlying superconducting mechanism may exist for different sub-families of the Fe-based superconductors (except for the $\text{K}_\alpha\text{Fe}_{2-\beta}\text{Se}_2$ series, where electron pockets instead of hole pockets are observed around the Γ point^{30,31}).

Despite the overall similarity, there are observable differences between the Fermi surface of the 10-3-8 phase and that of the prototype pnictides. In Fig. 4 we compare explicitly the in-plane ARPES Fermi surfaces for the 10-3-8 phase, BaFe_2As_2 (Ref. 32), and LaFeAsO (Ref. 33). First, the Dirac-cone-like Fermi dots around the X points in BaFe_2As_2 are absent in the 10-3-8 phase [seen most clearly in the 42 eV panel of Fig. 2(a)]. Since these dots are direct consequences of the long range antiferromagnetic order present in the 122 compound,^{32,34} their absence is consistent with the absence of an antiferromagnetic signature in transport measurements up to room temperature.² It is important to point out that the 10-3-8 phase is a superconductor, whereas no sign of superconductivity is found in BaFe_2As_2 . Related to the absence/presence of the Fermi dots near the X point, our

finding is consistent with the idea that superconductivity can be found in the iron pnictide compounds only if the in-plane electronic structure reduces to its paramagnetic appearance³² (except for the case of $\text{K}_\alpha\text{Fe}_{2-\beta}\text{Se}_2$). Second, extended ARPES intensity along one of the Γ - X_0 directions is seen only for the 10-3-8 phase. A close look into the k - E maps (data of Cut #3 in Fig. 2) reveals that there is a Fermi crossing in these locations, and that the band is holelike. We point out here that this band also originates from the Fe orbitals, since it shows reflective symmetry along the high symmetry directions of the iron unit cell rather than the triclinic platinum cell. Third, from the k_z dispersion data [Fig. 3(a)-(b)], one notices that ellipsoidal hole pockets are observed around both the Γ and Z_0 points for the 10-3-8 phase, while in the 122 parent compounds only Z ellipsoids are observed.^{27,28} According to band calculation (Fig. 5), this signifies the weak but existent Pt influence on the Fermi surface topology.

We now examine the electronic structure of the CaFePtAs system from the results of first principles calculations.^{18–20} In these calculations, spin-orbit coupling effects are not included and E_F is fixed assuming zero electron doping. The crystal structure of the 10-3-8 phase is taken from Ref. 2 with the off-plane Pt (Pt2) atom in the (Pt_3As_8) layer assigned to one of its two possible positions - slightly above the plane.² We show in Fig. 5(a) the calculated curves for the total density of states (DOS) as well as the partial DOS (PDOS) for the two different kinds of platinum atoms [Pt1 and Pt2, see Fig. 1(a)]. Similar to the prototype pnictides, the DOS in the vicinity of E_F for the 10-3-8 phase is dominated by Fe $3d$ orbitals. In Fig. 5(b)-(c), the calculated LDA band structure and Fermi surface are shown in the triclinic Brillouin zone. From Fig. 5(b) we see that the innermost Γ band has stronger k_z dispersion than the other two holelike iron bands, which is consistent with the ARPES observations [Fig. 3(a)-(c)]. This band is

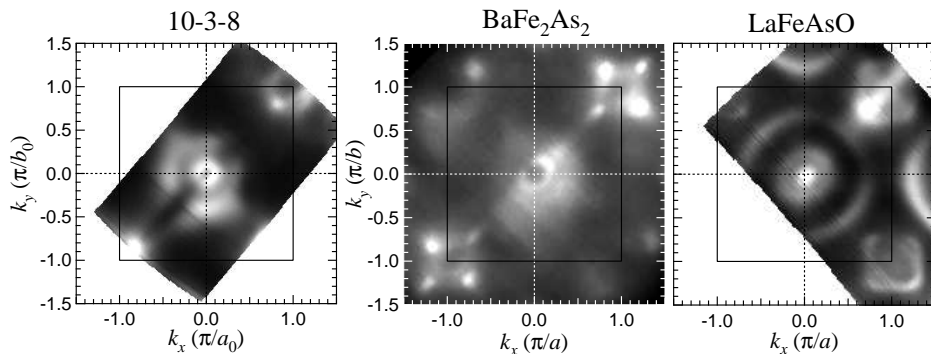


FIG. 4: Comparison of in-plane ARPES Fermi surfaces of the 10-3-8 phase, BaFe_2As_2 (Ref. 32), and LaFeAsO (Ref. 33). Incident photon energies are 22, 105, and 45 eV, respectively. The “Fermi dots” seen around the X pockets of BaFe_2As_2 come from antiferromagnetic reconstructions of the electronic structure,³² and the large Γ hole pocket in LaFeAsO originates from surface effects.³³

hybridized with the Pt d_{xz} orbitals. Since the experimental data reveal no sign of the triclinic Fermi surfaces, we assume that the potential from the $\sqrt{5}$ superlattice arising from the Pt_3As_8 layers is very weak, in which

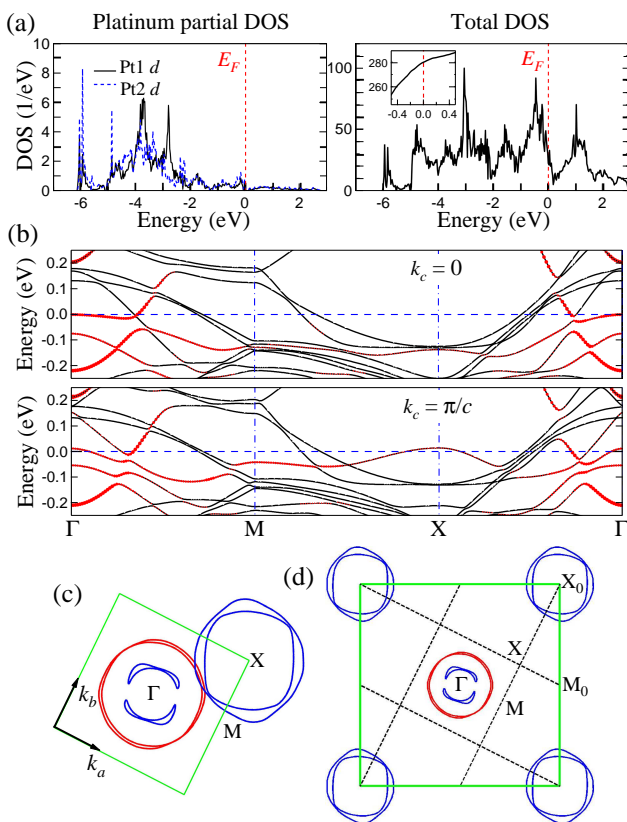


FIG. 5: (Color online) Results of first principles calculations. (a) Calculated density of states (DOS) for the 10-3-8 phase. Left column: partial DOS for in-plane and out-of-plane platinum 5d orbitals (Pt1 & Pt2, respectively). Right column: Total DOS for all elements. Inset shows the integrated DOS (IDOS) near E_F . (b) Calculated band structure of 10-3-8 in the triclinic Brillouin zone. Red (grey) dots indicate the contribution of platinum orbitals. (c) Fermi surfaces sketched in the triclinic zone. (d) Fermi surfaces unfolded into the tetragonal zone.

case we can approximately “unfold” the LDA superlattice band structure into the tetragonal BZ, as shown in Fig. 5(d). The tetragonal Γ , X_0 , and M_0 points form a subset of the supercell Γ , X , and M points. Therefore, we systematically “erase” all superlattice FS maps not associated with the tetragonal symmetry points. From Fig. 5(d), we see that this process works well for the Fe Fermi surfaces, reproducing the familiar 122 structure. The fate of the electronlike Pt-bands (the four pedal-like small pockets near Γ) under this unfolding process is less clear, but it should be noted that these pockets are not clearly distinguished by ARPES.

Interlayer hopping plays an important role in the presence of high- T_c superconductivity in both the cuprates and the Fe-based superconductors. It is believed that the hopping strength in the prototype pnictides is somewhat stronger than that in the cuprates (although still on the weak side), and that this may lead to the differences between T_c and pairing symmetry in these two families. Zhai *et al.* propose that the superconducting gap symmetry changes from d -wave to s -wave with increasing hopping strength.³⁵ Although the model in Ref. 35 may not apply directly to the Ca-Fe-Pt-As systems, where spin density wave signatures have not yet been detected at low temperatures, it is likely that the unique momentum-space separation of the inter- and intra-layer signals in the 10-3-8 system helps to determine the hopping strength with considerably higher accuracy, thus shedding light on the ultimate determination of the superconducting mechanism in both classes of high- T_c superconductors.

IV. CONCLUSION

In conclusion, we have presented a systematic study of the band structure and Fermi surfaces of one of the new Ca-Fe-Pt-As superconductors in the vicinity of E_F . Our ARPES observations, reduced tetragonal electronic structure and little k_z dispersion, point to a weak interlayer hopping strength in this system. The Dirac-cone-like Fermi dots around X are absent in the 10-3-8 phase, consistent with the absence of long range antiferromagnetism in this compound. First principle calcula-

tions agree well with experimental data if the potential from the $\sqrt{5}$ superlattice arising from the PtAs layers is considered to be very weak, and the triclinic band structure can be unfolded onto the tetragonal Brillouin zone. The Ca-Fe-Pt-As superconductors are ideal systems for the study of interlayer hopping in the iron-based superconductors. The present detailed study of the electronic structure of the 10-3-8 phase serves as an important step in that direction.

C. L. acknowledges T. Kondo and A. Kaminski for provision of data analysis software. Work at Princeton is supported by NSF-DMR-1006492 and the AFOSR MURI on superconductivity. The Synchrotron Radiation Center is supported by NSF-DMR-0537588. Work at Northeastern and Princeton is supported by the Basic Energy Sciences, U.S. Department of Energy (DE-FG02-07ER46352, DE-FG-02-05ER46200, and AC03-76SF00098), and benefited from the allocation of supercomputer time at NERSC and Northeastern University's Advanced Scientific Computation Center. M. Z. H. acknowledges Visiting Scientist support from LBNL and additional support from the A. P. Sloan Foundation.

- ¹ K. Kudo *et al.*, International workshop on novel superconductors and super materials, March 6-8, Tokyo, Japan (2011).
- ² N. Ni, J. M. Allred, B. C. Chan, and R. J. Cava, Proc. Natl. Acad. Sci. **108**, E1019-E1026 (2011).
- ³ C. Lohmert, T. Stürzer, M. Tegel, R. Frankovsky, G. Friederichs, and D. Johrendt, Angew. Chem. Int. Ed. **50**, 9195-9199 (2011).
- ⁴ S. Kakiya, K. Kudo, Y. Nishikubo, K. Oku, E. Nishibori, H. Sawa, T. Yamamoto, T. Nozaka, and M. Nohara, J. Phys. Soc. Jpn. **80**, 093704 (2011).
- ⁵ Y. Kamihara, T. Watanabe, M. Hirano, and H. Hosono, J. Am. Chem. Soc. **130**, 3296 (2008).
- ⁶ M. Rotter, M. Tegel and D. Johrendt, Phys. Rev. Lett. **101**, 107006 (2008).
- ⁷ X. C. Wang, Q. Q. Liu, Y. X. Lv, W. B. Gao, L. X. Yang, R. C. Yu, F. Y. Li, and C.Q. Jin, Solid State Commun. **148**, 538 (2008).
- ⁸ F.-C. Hsu, J.-Y. Luo, K.-W. Yeh, T.-K. Chen, T.-W. Huang, P. M. Wu, Y.-C. Lee, Y.-L. Huang, Y.-Y. Chu, D.-C. Yan, and M.-K. Wu, Proc. Natl. Acad. Sci. USA **105**, 14262 (2008).
- ⁹ J. Guo, S. Jin, G. Wang, S. Wang, K. Zhu, T. Zhou, M. He, and X. Chen, Phys. Rev. B **82**, 180520(R) (2010).
- ¹⁰ D. C. Johnston, Adv. Phys. **59**, 803 (2010).
- ¹¹ P. C. Canfield, S. L. Bud'ko, N. Ni, J. Q. Yan, and A. Kracher, Phys. Rev. B **80**, 060501(R) (2009).
- ¹² N. Ni and S. L. Bud'ko, MRS bulletin, **36**, 620 (2011).
- ¹³ J. G. Bednorz and K. A. Müller, Z. Phys. B **64**, 189 (1986).
- ¹⁴ D. M. Ginsberg, Physical Properties of High Temperature Superconductors Vol. V. World Scientific Pub. Co. Inc. ISBN: 978-9810233587 (1996).
- ¹⁵ A. Mourachkine, High-temperature superconductivity in cuprates: the nonlinear mechanism and tunneling measurements. Springer ISBN: 978-1402008108 (2002).
- ¹⁶ A. Damascelli, Z. Hussain and Z.-X. Shen, Rev. Mod. Phys. **75**, 473 (2003).
- ¹⁷ J. C. Campuzano, M. Norman, and M. Randeria, Superconductivity: Physics of Conventional and Unconventional Superconductors, Vol. 1, edited by K. H. Bennemann and J. B. Ketterson (Springer, Berlin, 2008).
- ¹⁸ G. Kresse, and J. Joubert, Phys. Rev. B **59**, 1758 (1999).
- ¹⁹ P. E. Blöchl, Phys. Rev. B **50**, 17953 (1994).
- ²⁰ G. Kresse and J. Furthmüller, Comput. Mater. Sci. **6**, 15 (1996).
- ²¹ H. Ding, P. Richard, K. Nakayama, K. Sugawara, T. Arakane, Y. Sekiba, A. Takayama, S. Souma, T. Sato, T. Takahashi, Z. Wang, X. Dai, Z. Fang, G. F. Chen, J. L. Luo, and N. L. Wang, EPL **83**, 47001 (2008).
- ²² L. Zhao, H.-Y. Liu, W.-T. Zhang, J.-Q. Meng, X.-W. Jia, G.-D. Liu, X.-L. Dong, G.-F. Chen, J.-L. Luo, N.-L. Wang, W. Lu, G.-L. Wang, Y. Zhou, Y. Zhu, X.-Y. Wang, Z.-Y. Xu, C.-T. Chen, and X.-J. Zhou, Chin. Phys. Lett. **25**, 4402 (2008).
- ²³ L. Wray, D. Qian, D. Hsieh, Y. Xia, L. Li, J. G. Checkelsky, A. Pasupathy, K. K. Gomes, C. V. Parker, A. V. Fedorov, G. F. Chen, J. L. Luo, A. Yazdani, N. P. Ong, N. L. Wang, and M. Z. Hasan, Phys. Rev. B **78**, 184508 (2008).
- ²⁴ V. B. Zabolotnyy, D. S. Inosov, D. V. Evtushinsky, A. Koitzsch, A. A. Kordyuk, G. L. Sun, J. T. Park, D. Haug, V. Hinkov, A. V. Boris, C. T. Lin, M. Knupfer, A. N. Yaresko, B. Büchner, A. Varykhalov, R. Follath, and S. V. Borisenko, Nature **457**, 569 (2009).
- ²⁵ P. Richard, T. Sato, K. Nakayama, S. Souma, T. Takahashi, Y.-M. Xu, G. F. Chen, J. L. Luo, N. L. Wang, and H. Ding, Phys. Rev. Lett. **102**, 047003 (2009).
- ²⁶ A. Koitzsch, D. S. Inosov, D. V. Evtushinsky, V. B. Zabolotnyy, A. A. Kordyuk, A. Kondrat, C. Hess, M. Knupfer, B. Büchner, G. L. Sun, V. Hinkov, C. T. Lin, A. Varykhalov, and S. V. Borisenko, Phys. Rev. Lett. **102**, 167001 (2009).
- ²⁷ C. Liu, T. Kondo, N. Ni, A. D. Palczewski, A. Bostwick, G. D. Samolyuk, R. Khasanov, M. Shi, E. Rotenberg, S. L. Bud'ko, P. C. Canfield, and A. Kaminski, Phys. Rev. Lett. **102**, 167004 (2009).
- ²⁸ T. Kondo, R. M. Fernandes, R. Khasanov, C. Liu, A. D. Palczewski, N. Ni, M. Shi, A. Bostwick, E. Rotenberg, J. Schmalian, S. L. Bud'ko, P. C. Canfield, and A. Kaminski, Phys. Rev. B **81**, 060507(R) (2010).
- ²⁹ H. Ding, K. Nakayama, P. Richard, S. Souma, T. Sato, T. Takahashi, M. Neupane, Y.-M. Xu, Z.-H. Pan, A. V. Fedorov, Z. Wang, X. Dai, Z. Fang, G. F. Chen, J. L. Luo, and N. L. Wang, J Phys. Condens. Matter **13**, 135701 (2011).
- ³⁰ Y. Zhang, L. X. Yang, M. Xu, Z. R. Ye, F. Chen, C. He, H. C. Xu, J. Jiang, B. P. Xie, J. J. Ying, X. F. Wang, X. H. Chen, J. P. Hu, M. Matsunami, S. Kimura, and D. L. Feng, Nature Materials **10**, 273 (2011).
- ³¹ T. Qian, X.-P. Wang, W.-C. Jin, P. Zhang, P. Richard, G. Xu, X. Dai, Z. Fang, J.-G. Guo, X.-L. Chen, and H. Ding, Phys. Rev. Lett. **106**, 187001 (2011).
- ³² C. Liu, T. Kondo, R. M. Fernandes, A. D. Palczewski, E.-D. Mun, N. Ni, A. N. Thaler, A. Bostwick, E. Rotenberg, J. Schmalian, S. L. Bud'ko, P. C. Canfield, and A. Kaminski, Nature Physics **6**, 419 (2010).
- ³³ C. Liu, Y. Lee, A. D. Palczewski, J.-Q. Yan, T. Kondo, B. N. Harmon, R. W. McCallum, T. A. Lograsso, and A. Kaminski, Phys. Rev. B **82**, 075135 (2010).
- ³⁴ Y. Xia, L. Wray, D. Qian, D. Hsieh, H. Lin, A. Bansil, D. Grauer, Y. Hor, R. J. Cava, and M. Z. Hasan, Nature Physics **5**, 398-402 (2009); D. Hsieh, D. Qian, L. Wray, Y. Xia, Y. Hor, R. J. Cava, and M. Z. Hasan Nature **452**, 970 (2008); M. Z. Hasan and B. A. Bernevig, Physics **3**, 27 (2010).
- ³⁵ H. Zhai, F. Wang, and D.-H. Lee, Phys. Rev. B **80**, 064517 (2009) and references therein.